Applied Catalysis B: Environmental 183 (2016) 185–196

Contents lists available at ScienceDirect

Applied Catalysis B: Environmental

journal homepage: www.elsevier.com/locate/apcatb

Repercussion of the carbon matrix for the activity and stability of Fe/N/C electrocatalysts for the oxygen reduction reaction

Carlota Domínguez [a], Francisco José Pérez-Alonso [a,*], Mohamed Abdel Salam [b], Shaeel A. Al-Thabaiti [b], Miguel Antonio Peña [a], F. Javier García-García [c], Laura Barrio [a], Sergio Rojas [a,*]

[a] Grupo de Energía y Química Sostenibles, Instituto de Catálisis y Petroleoquímica, CSIC, C/Marie Curie 2, 28049 Madrid, Spain
[b] Chemistry Department, Faculty of Science, King Abdulaziz University, PO Box 80200, Jeddah 21589, Saudi Arabia
[c] Centro Nacional de Microscopía, Universidad Complutense de Madrid, Madrid, Spain

ARTICLE INFO

Article history:
Received 17 August 2015
Received in revised form 15 October 2015
Accepted 21 October 2015
Available online 26 October 2015

Keywords:
Fuel cells
Oxygen reduction reaction
Graphene
Iron
Durability

ABSTRACT

Graphene-like (G), multiwalled carbon nanotubes (CNTs) and active carbon (AC) have been used as carbon matrix for the synthesis of Fe/N/C catalysts for the oxygen reduction reaction. A thorough physicochemical characterization of the electrocatalysts, including X-ray photoelectronic and X-ray absorption spectroscopies, reveal that the formation of Fe/Nx ensembles is favored when the graphene-like or the CNTs are used as the carbon matrix. As a result, the catalyst prepared with the graphene matrix (Fe/N/G) records the highest activity for the ORR in the series of 3.1 A g^{-1} at 0.9 V. This very high ORR activity positions these catalysts as a realistic alternative to replace Pt/C cathodes in alkaline fuel cells. Moreover, using graphene as the carbon matrix endows the catalyst with very high stability during the ORR showing stable catalytic performance for the ORR even after being subjected to severe treatments of 3000 cycles up to 1.4 V. *In situ* IRRA spectra demonstrate that such a high stability for the ORR relates to the excellent resistance against corrosion of the graphene-based catalyst.

1. Introduction

The increasing growth of energy consumption, which is mainly coped with fossil fuels, is causing severe environmental and social issues including climate change, geopolitical tensions and concerns about fossil fuel depletion. As a consequence, numerous efforts to find alternative energy sources, especially renewable ones, have been addressed during the last years. Electrochemical devices such as fuel cells [1] and metal–air batteries [2] are expected to power environmentally friendly vehicles in a near future. Some of the most relevant environmentally friendly energy related processes such as the hydrogen evolution reaction (HER), the hydrogen oxidation reaction (HOR), the oxygen evolution reaction (OER) and the oxygen reduction reaction (ORR), are conducted in the presence of electrocatalysts [3,4] which usually contain high amounts of scarce and expensive Platinum group metals (PGM). The urgent and great challenge is to design and develop highly active and more durable electrocatalysts based upon low cost, earth-abundant elements with comparable activity to that of the benchmark PGM based catalysts [5]. In recent times, non-precious metal catalysts (NPMCs) based upon the incorporation of transition metals such as Fe onto N/C composites (usually denoted as Fe/N/C) have emerged as the most suitable candidates for replacing Pt as electrocatalysts for the ORR in Proton Exchange Membrane Fuel Cells (PEMFC) [6–15]. The lower kinetics of this type of NPMCs for the ORR can be compensated by using higher NPMCs loadings without economic penalties [7,13]. Moreover, in the last years, NPMCs with comparable ORR kinetic currents in acid media than that obtained with benchmark carbon supported PGM have been reported [8,11,12,16]. The results are even more promising in alkaline media and several groups have developed electrocatalysts based upon Fe/N/C structures [17,18] with ORR activity that match, or even exceed, the activity of Pt/C.

Although the actual nature of the active sites for the ORR in Fe/N/C catalysts remains elusive it is well accepted that their activity increases when Fe atoms are coordinated to the N heteroatoms incorporated onto the C-C sp^2 network of a carbon matrix, usually

* Corresponding authors.
E-mail addresses: fperez@icp.csic.es (F.J. Pérez-Alonso), srojas@icp.csic.es (S. Rojas).

http://dx.doi.org/10.1016/j.apcatb.2015.10.043
0926-3373/

active carbon [9,13,19,20]. In addition, it is also proposed that the formation of the active sites takes place inside the micropores of the carbon network [21], resulting in catalysts with high active surface area. However, the presence of micropores results in severe mass transportation limitations when high current densities are demanded to PEMFCs [8].

The state-of-the-art mesoporous carbon supports used in the cathodes of fuel cells are prone to suffer severe corrosion phenomena due to the strong oxidizing environment in the cathode electrode of PEMFCs. Due to their special 1D and 2D structures, carbon nanotubes and graphene-based materials possess unique properties such as high conductivity, high surface area and stability [10,22,23], thus being very attractive alternative carbon matrixes or supports for the synthesis of electrocatalysts. Several works have explored the use of nitrogen-doped graphene and/or carbon nanotubes as supports for the synthesis electrocatalysts for the ORR, resulting in more active and stable electrocatalysts for the ORR [9,10,17,18,22,24–28]. Despite the utter importance of the carbon matrix for the synthesis and performance of the Fe/N/C catalysts for the ORR, there is a lack of systematic studies addressing this issue. It seems to be widely accepted that the activity of Fe/N/C based catalysts for the ORR increases by using graphene like or carbon nanotubes or even carbon nanotube-graphene complexes as the carbon matrix [9,13,17]. However, it has been recently reported that the activity for the ORR in KOH of Fe/N/C-based catalysts prepared with high area carbon black is significantly higher than when prepared with graphene nanosheets [18].

In this work we explore the effect of the carbon matrix for the synthesis and catalytic performance of Fe/N/C catalysts by preparing series of catalysts using the same Fe and N precursors, but different types of carbons, namely graphite nanoplates (graphene, G), multiwalled carbon nanotubes (CNTs) or active carbon (AC). The formation of Fe/Nx-like ensembles is favoured when CNTs or graphene are used as support. The catalyst prepared with graphene, Fe/N/G, exhibits very high ORR activity in alkaline electrolyte which compares well against that of Pt/C benchmark catalyst. Equally important, this catalyst displays an outstanding stability against corrosion in alkaline media after repeated cycling up to 1.4 V *vs.* RHE.

2. Experimental

2.1. Synthesis of catalyst

The following commercially available carbons are used for the synthesis of the catalysts: Graphene (graphite nanoplates, from XG Sciences, Grade C), multiwalled carbon nanotubes (from Nanocyl) and active carbon (Norit GSX). The catalysts studied in this work were synthesized by a series of sequential ballmilling steps in a 12 mL stainless steel vessel followed by pyrolysis at 800 °C. In a first step, 0.75 g of the desired carbon matrix and 0.0027 g of the N precursor (1,4,8,11-tetraazacyclo-tetradecane, Aldrich 98%) were ballmilled at 350 rpm during 4 h. The N/C composite obtained was mixed with 0.75 g of the same carbon material than that used in the previous step and 1.3 g of Urea (CH_4N_2O, Panreac, PRS) and ballmilled at 350 rpm during 4 h. The N/C composite obtained was mixed with 0.52 g of iron phthalocyanine (Aldrich) and ballmilled for 10 h. The solid obtained was thermally treated (pyrolised) in a quartz tubular reactor at 800 °C for 30 min in an atmosphere of 50 mL min^{-1} of NH_3 (5%)/Ar. The catalysts obtained are labelled as Fe/N/G, Fe/N/CNT or Fe/N/AC where G, CNT and AC are used to identify graphene, carbon nanotubes or active carbon, respectively. Note that Fe/N/C will be used as a generic term to identify the family of Fe/N-based catalysts reported in this work irrespectively of the actual carbon matrix

2.2. Physicochemical characterization

X-ray photoelectron spectra (XPS) were acquired with a SPECS customized system for surface analysis equipped with a non-monochromatic X-ray source XR 50 and a hemispherical energy analyser PHOIBOS 150. X-ray MgKα line (1253.6 eV) was used as excitation (operating at 200 W/12 kV), and the medium area mode of the lenses was used for the detector. The energy regions of the photoelectrons of interest were scanned at increments of 0.1 eV and fixed pass energy of 25 eV until an acceptable signal-to-noise ratio was achieved. Atomic abundances were estimated by calculating the integral of each peak, determined by subtraction of the Shirley-type background and fitting of the experimental curve to a combination of Lorentzian and Gaussian using the appropriate sensitivity factors for each element [29]. Binding energies (±0.2 eV) were determined by setting the C 1s peak at 284.6 eV.

C, H and N contents of the samples were measured with an elemental analyser (LECO CHNS-932). Total iron content of the catalysts was analysed by inductively coupled plasma with an ICP–OES Optima 3300DV (PerkinElmer) after acidic microwave digestion of the samples.

Textural properties were evaluated by N_2 adsorption–desorption isotherms of the samples recorded at liquid N_2 temperature with a Micromeritics ASAP 2000 apparatus. Samples were degassed at 140 °C under vacuum for 24 h. Specific areas were calculated by applying the BET method within the relative pressure range $P/P^0 = 0.05–0.30$.

XAFS data were acquired at CLAESS beam line at ALBA Synchrotron facility with the help of ALBA staff. A Si (1 1 1) double crystal monochromator working in continuous mode was used for the energy scans. Fe K absorption edge (7112 eV) was calibrated with the help of a Fe foil, placed between second and third ionization chambers, and measured simultaneously with the sample spectra. Catalysts samples were pressed in self-supporting pellets. The spectra were recorded in the transmission mode at ambient temperature. EXAFS spectra are the result of the merge of at least 6 scans. The following selected standard materials were analyzed: Fe foil, Fe_3O_4, Fe_3C and iron phthalocyanine (FePhC). The analysis of the EXAFS spectra was performed with the software VIPER for Windows. In the spectra of the absorption coefficient μ, a linear fit was made to the pre-edge region in order to normalize the signal. A smooth atomic background μ_0 was evaluated using a smoothing cubic spline [30].

TEM and STEM images were recorded with at TEM/STEM JEOL 2100F microscope operated at 200 kV. The microscope was equipped with an OXFORD INCA detector for EDS analyses. Specimens for TEM analyses were prepared by dispersing the catalysts in butanol and placing one drop onto a holey-carbon-coated copper supported grid.

2.3. Electrochemical tests

The electrochemical tests were performed with a computer controlled Autolab Pgstat 302N potentiostat/galvanostat. A standard three-compartment glass cell and a rotating disk electrode (RDE) (Pine research instruments) were used for all electrochemical experiments. The counter electrode was a graphite rod and the reference electrode was a Reversible Hydrogen Electrode (RHE). A glassy carbon electrode with a thin film of the electrocatalyst under study was used as the working electrode. The electrocatalyst was deposited on the electrode by means of an ink prepared by ultrasonically dispersing 6 mg of the catalyst in 800 μL of water, 200 μL of isopropyl alcohol and 20 μL of 5 wt.% Nafion. 20 μL of the ink were deposited on the electrode resulting in a catalyst loading of 0.6 mg_{cat} cm^{-2}. Previous to the electrochemical testing, the work-

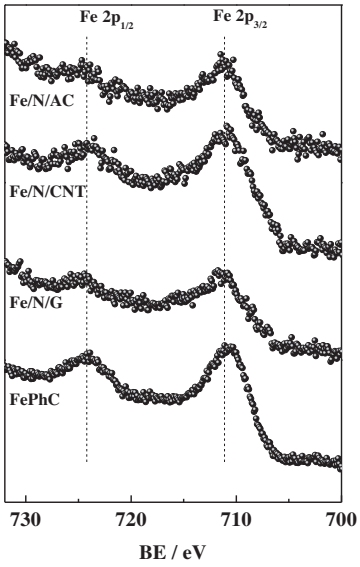

Fig. 1. Fe 2p core-level spectra of Fe/N/G, Fe/N/CNT and Fe/N/AC. The spectrum for iron phthalocyanine (FePhC) is shown for comparison.

ing electrode was cleaned by potential cycling from 0 to 1.1 V for 50 cycles in Ar-saturated electrolyte: 0.1 M KOH or 0.1 M $HClO_4$.

The ORR polarization curves were collected at 10 mV s^{-1} and 1600 rpm between 0.0 and 1.2 V or 0.0 and 1.0 V in O_2 saturated 0.1 M KOH or 0.1 M $HClO_4$ electrolytes, respectively. The Faradaic current density (j_F mA cm^{-2}) was obtained by subtracting the current obtained during the anodic sweep in the O_2 saturated electrolyte from the capacitive current recorded in Ar-saturated electrolyte under the same experimental conditions.

H_2O_2 production was evaluated by using a rotating ring disk electrode (RRDE) (with a Pt ring), under the same experimental conditions than that reported above for the RDE applying a constant ring potential of 1.2 V. The fraction of H_2O_2 produced was calculated as shown in Eq. (1) [31],

$$X_{H_2O_2} = \frac{\frac{2i_R}{N}}{i_D + \frac{i_R}{N}} \quad (1)$$

where i_D is the disk current and i_R is the ring current. Ring efficiency (N) is of 26%.

The number of exchanged electrons was calculated from Eq. (2).

$$ne = 4 - \left(\frac{\%H_2O_2}{50\%}\right) \quad (2)$$

The ORR kinetic current (i_k) was calculated from the Koutecky–Levich equation as shown in Eq. (3)

$$i_k = -\frac{i_F \times i_{lim}}{i_F - i_{lim}} \quad (3)$$

where i_k is the kinetic current defined as <0 for reduction reactions and i_{lim} is the limiting current. Finally, the ORR mass activity is defined in Eq. (4),

$$i_m = -\frac{i_k}{m_{cat}} \quad (4)$$

where m_{cat} is the catalyst loading in grams [6].

For the stability tests simulating fuel cell operation, the working electrode was cycled between 0.6 and 1.0 V at 50 mV s^{-1} for 3000 cycles in O_2 saturated electrolyte without rotation. With the aim of simulating the severe oxidizing environments during start-up and stop cycles of a fuel cell, the working electrode was cycled between 0.4 and 1.4 V at 1 V s^{-1} for 3000 cycles in O_2 saturated electrolyte without rotation. The ORR polarization curves were collected before and after the stability tests following the procedure described above.

In situ electrochemical IRRAS studies of the corrosion of Fe/N/C catalysts were performed with a NICOLET 6700 FT-IR spectrometer equipped with a MCT detector and fitted with a PIKE Technologies VeeMAX II spectroscopic accessory. A poly (methyl methacrylate) (PMMA) cell with a CaF_2 prism bevelled at 60° at its bottom was used. FTIR spectra were acquired from the average of 64 interferograms, obtained with 4 cm^{-1} resolution at selected potential, by applying single potential steps from a reference potential (E_0 = 0.6 V *vs.* RHE) in the positive direction up to 1.4 V. The reflectance ratio R/R_0 was calculated, where R and R_0 are the reflectance measured at the sample and the reference potential, respectively. Electrochemical control was carried out using an Autolab PGstat 302 N.

3. Results and discussion

3.1. Catalyst characterization

The H, C, N and Fe contents of the Fe/N-based electrocatalysts as determined by elemental analysis (H, C and N) and ICP-OES analysis (Fe content) are reported in Table 1. The amount of nitrogen incorporated into the catalysts are of 2.8, 2.6 and 2.3 wt.% for Fe/N/G, Fe/N/AC and Fe/N/CNT, respectively. These similar values suggest that the amount of nitrogen actually incorporated into the catalysts is not strongly influenced by the nature of the carbon material used for the synthesis of the catalysts.

Table 1 also shows the BET, micropore and external surface area values obtained from the N_2 adsorption–desorption isotherms. In all cases, the BET surface area of the catalysts is smaller than that of the pristine carbon material of 718, 233 and 850 m^2 g^{-1}, for graphene, CNT and AC, respectively.

The surface composition of the catalysts was studied by XPS. Table 2 shows the relative abundance of Fe, C and N as calculated from X-ray photoelectron spectroscopy of the Fe/N-based catalysts.

All catalysts have similar N/C contents ranging between 0.021 for Fe/N/G and 0.026 or 0.028 for Fe/N/CNT and Fe/N/AC, respectively. These values are in good agreement with the atomic ratios derived from the elemental analysis indicating the lack of N segregation onto catalyst surface. In order to identify and quantify the N atoms incorporated into the C-C network, the N 1s core-level spectra were analysed (Fig. S1 in Supplementary material). The peaks

Table 1
Weight contents and specific surface areas of the catalysts.

Catalyst	C (wt.%)	H (wt.%)	N (wt.%)	Fe (wt.%)	BET (m^2 g^{-1})
Fe/N/G	86.4	0.7	2.8	2.4	415 (162/253)
Fe/N/CNT	89.0	0.5	2.3	2.0	166 (21/145)
Fe/N/AC	83.6	1.1	2.6	2.4	362 (164/198)

C, H, and N wt.% as determined from elemental analysis; Fe wt.% as determined from ICP-OES analyses. Specific surface areas determined form the BET method. The values in parentheses indicate micropore/external areas.

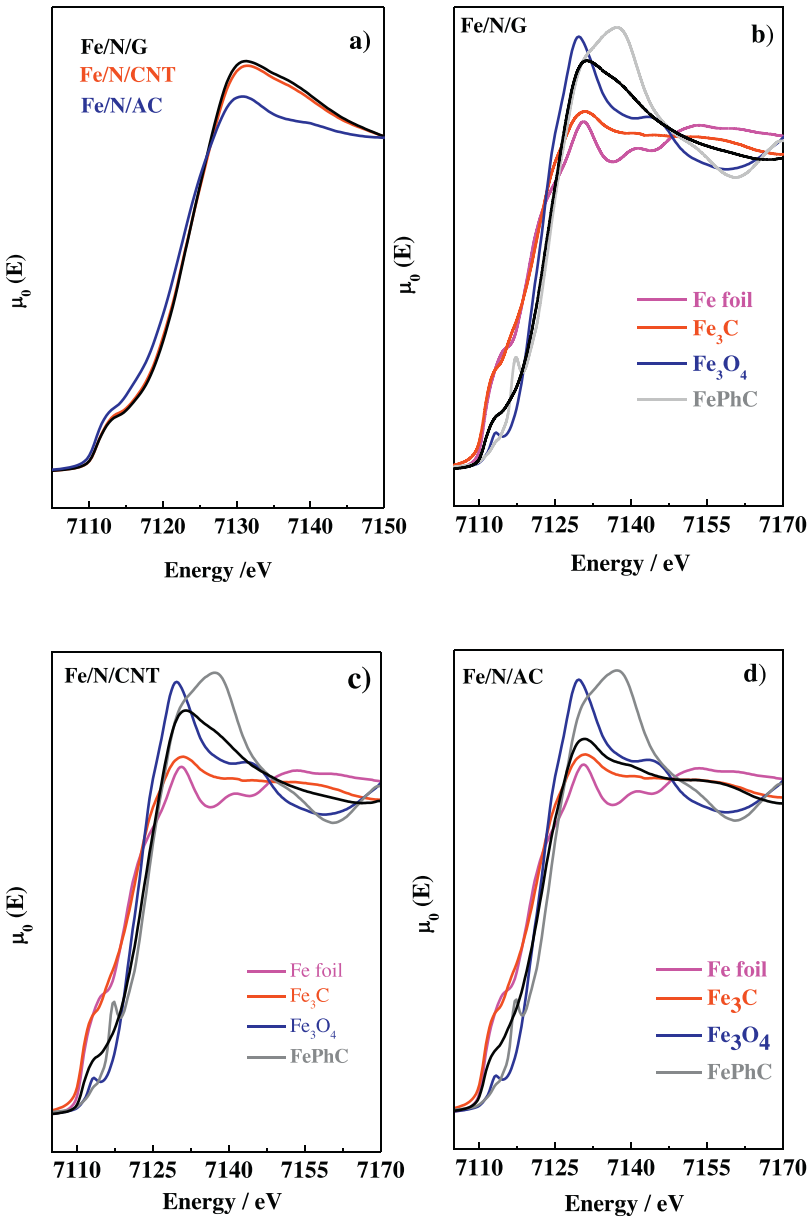

Fig. 2. (a) Fe K-edge XANES spectra of Fe/N/G, Fe/N/CNT and Fe/N/AC. (b), (c) and (d) XANES spectrum of each catalyst compared with the spectra of the standard materials.

were fitted to four components with peak maxima at 398.5, 400.1, 401.0–401.5 and 402–405 eV and assigned to pyridinic-N, pyrrolic-N, graphitic-N species and oxide-N, respectively [6,32]. As shown in Table 1, the relative amount of the N species, *i.e.*, pyridinic-N pyrrolic-N, graphitic-N and oxide-N species is similar in all catalysts regardless of the nature of the carbon matrix. Pyridinic-N is the predominant species in all catalysts, followed by pyrrolic-N and graphitic-N.

Fig. 1 shows the Fe 2p core-level spectra of the Fe/N/C electrocatalysts. All spectra show a broad peak centred at *ca.* 711 eV which is usually ascribed to the presence of iron oxidized species, typically Fe^{2+} or/and Fe^{3+}. The precise assignment of this peak is usually done from the position of the characteristic shake-up satellite peaks of

Table 2
Surface elemental chemical composition.

Sample	Surface atomic content			Relative atomic amount of N species			
	N/C	O/C	Fe/C	Pyridinic	Pyrrolic	Graphitic	Oxide
Fe/N/G	0.021 (0.028)	0.050	0.0018 (0.0060)	0.46	0.32	0.19	0.03
Fe/N/CNT	0.026 (0.022)	0.034	0.0028 (0.0048)	0.51	0.32	0.11	0.06
Fe/N/AC	0.028 (0.027)	0.090	0.0023 (0.0062)	0.46	0.32	0.17	0.05

N/C, Fe/C and O/C surface atomic ratios and relative atomic amount of N species derived from XPS analyses; for the sake of comparison bulk N/C and Fe/C atomic ratios (from Table 1) are shown in parentheses.

these iron species [33]. However, the spectra shown in Fig. 1 lack of the characteristic, well defined, satellite peaks for Fe^{2+} (at *ca.* 715 eV) or Fe^{3+} (at *ca.* 719 eV) species in oxide structures. This feature is indicative of the presence of Fe_3O_4 [34,35] and/or of iron phthalocyanine (spectrum also shown in Fig. 1). The surface concentration of Fe in the catalysts (see Fe/C atomic ratio in Table 2) is of *ca.* 0.002 for Fe/N/G and Fe/N/AC and slightly higher in Fe/N/CNT (Fe/C = 0.0028). As also shown in Table 2, the surface concentration of iron (Fe/C = 0.0018–0.0028) is indeed lower than the bulk concentration (Fe/C = 0.0048–0.0062). This feature indicates that a significant fraction of the iron atoms (of around 66%) is not exposed at the catalyst surface suggesting Fe atoms become covered by several carbon layers during the synthesis of the catalysts.

The nature of the iron species and their electronic state was further studied by X-ray absorption spectroscopy. The XANES and EXAFS spectra of the catalysts are shown in Figs. 2 and 3 respectively. For the sake of comparison, the XANES and EXAFS spectra of selected standards: Fe foil, Fe_3O_4, Fe_3C and iron phthalocyanine (FePhC), are also shown. The Fe K-edge XANES spectra for Fe/N/G and Fe/N/CNT are almost identical showing no significant shifts of the absorption edge positions. However, the spectra for Fe/N/AC is slightly different showing an evident shift to lower energy which can be taken as a clear indication of the different electronic state of the Fe atoms in Fe/N/AC as compared to Fe/N/G or Fe/N/CNT. The XANES spectra for each catalyst are compared with the spectra of the standard materials in Fig. 2b–d. The shifting of the adsorption edge of the Fe species in Fe/N/AC could be indicative of the presence of Fe_3C or Fe^0 (as in Fe foil) species in this catalyst. A careful inspection of the energy region of the spectra between 7130 and 7170 eV by analysing its first derivative shows that the iron species in Fe/N/AC are more similar to Fe_3C than to Fe foil. On the other hand, the adsorption edge of Fe in Fe/N/G and Fe/N/CNT is closer to that recorded for FePhC or Fe_3O_4.

A careful inspection of the energy region of the spectra between 7158 and 7170 eV shows that the iron species in Fe/N/G and Fe/N/CNT are more similar to those in FePhC than in Fe_3C.

The phase uncorrected interatomic distances obtained by Fourier transformation of the EXAFS spectra over the k-space range between 3 and 14.5 $Å^{-1}$ of the catalysts studied in this work along with the signals for the Fe foil, Fe_3O_4, Fe_3C and FePhC standard materials are shown in Fig. 3. As observed, the most intense peak in the spectra for all catalysts is centred at *ca.* 2.1 Å. However, this peak is asymmetric and the contribution from another peak at *ca.* 1.6 Å is evident, especially in the spectra for Fe/N/G and Fe/N/CNT. The first peak is consistent with a Fe—N or Fe—O distance, while the second peak corresponds to the first shell Fe-Fe distance in the metal foil or carbide phases. The intensity of the peak (shoulder) at ca. 1.6 Å is significantly smaller in the spectrum of Fe/N/AC. The most intense peaks in the spectra of the standard materials appear at *ca.* 1.6 (Fe_3O_4, FePhC, shoulder in Fe_3C), 2.1 (Fe foil, Fe_3C), 2.7 (Fe_3O_4), and 4.4 (Fe foil) Å.

The peak at 1.6 Å can be assigned to the distances Fe—C (Fe_3C), Fe—N (FePhC) and Fe—O (Fe_3O_4), whereas the rest of the peaks correspond to the distance FeFe in Fe foil 1st shell (2.1 Å), Fe_3C (2.1 Å), Fe_3O_4 (2.7 Å) and Fe foil 2nd shell (4.4 Å) [36–39].

The local structure of Fe in the catalysts under study resembles to that of the Fe_3C standard showing a peak at 2.1 Å (distance Fe—Fe) and shoulder at ca. 1.6 Å (distance Fe—C), indicating that Fe_3C is the most abundant iron phase in the catalysts (Fig. 3). However, the intensity of the peak at 1.6 Å in the spectra for Fe/N/G and Fe/N/CNT is almost the same than that of the main peak at *ca.* 2.1 Å suggesting that other iron species are present in these catalysts. As shown in Fig. 3, the peak at 1.6 Å is characteristic of Fe—N or Fe—O distances; however the presence latter species should be ruled out because the spectra for the catalysts lack of the most intense peaks at *ca.* 2.5 and 3.0 Å which are clearly observed in the spectra of

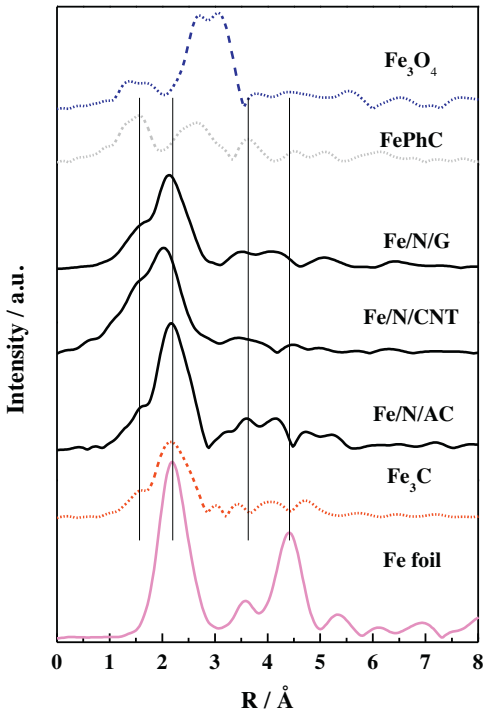

Fig. 3. FT EXAFS spectra for samples Fe/N/G, Fe/N/CNT and Fe/N/AC. Spectra of Fe foil, Fe_3O_4, Fe_3C and iron phthalocyanine (FePhC) are included for comparison.

the Fe_3O_4 standard. The formation of Fe_3N upon thermal treatments in highly concentrated NH_3 (>60 vol.%) has been proposed by other authors [40]. These phases are not protected by graphitic layers and can be passivated after air exposure forming Fe—O bonds. However, we found no evidences of the formation of iron nitride (Fe_3N) crystalline phases in our catalysts. Fig. S2 shows the X-ray diffractograms for the Fe/N/C catalysts (and for the pristine carbons). Although several diffraction lines for Fe_3C and Fe_3N appear at similar 2 theta values, the presence of small peaks between 48 and 49° along with the stronger diffraction line at 45° indicate the presence of Fe_3C. On the other hand, the most intense peak for Fe_3N at 43.55° is not observed in the diffractograms of the Fe/N/C catalysts. It should be noted that the small diffraction peak at 43.8° in the diffractograms for the Fe/N/C coincides better with the diffraction line for Fe_3C at 43.86° than with the one for Fe_3N at 43.55°. In fact, the absence of iron nitrides phases could be due to the low volume percentage of NH_3 (5%) used in the pyrolysis step during the synthesis of the Fe/N/C catalysts reported in this work, (see Section 2). As a consequence, the peak at 1.6 Å is assigned to Fe—N distance similar to those found in FePhc that are present in Fe/N/G and Fe/N/CNT. It should be noted that the Fe—N species in these catalysts are not identical to those in the Fe-phthalocyanine used as reference; the X-ray absorption spectra clearly indicate the formation of FeNx species in the catalysts. The abundance of these FeNx-like species is higher in Fe/N/G and Fe/N/CNT than in Fe/N/AC, which is mainly composed by Fe_3C-like iron species. This conclusion is also supported by the XANES (Fig. 2), where the Fe absorption edge of Fe/N/G and Fe/N/CNT is shifted toward higher energies. However, the formation of Fe—O bonds in the surface of the carbon matrix can be produced in a small extend, and it is compatible with the EXAFS spectroscopic results.

As shown above, Fe_3C species were not detected by XPS (neither in the Fe 2p nor in the C 1s core-level regions) indicating that such Fe_3C species are encapsulated within the carbon matrix rather than exposed at the catalyst surface. This conclusion is in line with the surface and bulk Fe/C atomic ratios calculated from XPS and

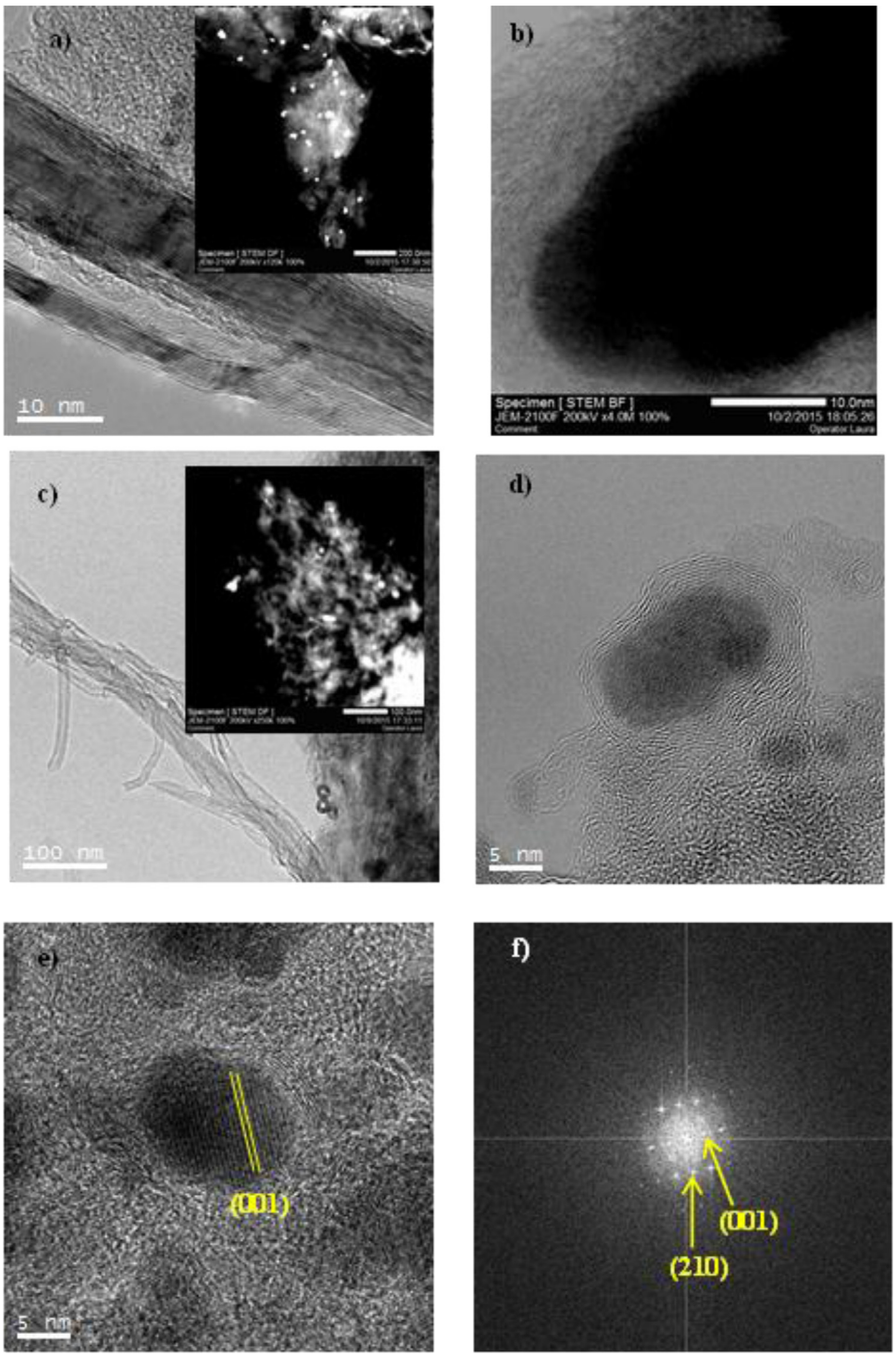

Fig. 4. (a) and (b) TEM and STEM (bright field) images of Fe/N/G. The inset to figure (a) is a STEM image for Fe/N/G. (c) and (d) TEM images of Fe/N/CNT. The inset to figure (c) is a STEM image for Fe/N/CNT. (e) HR-TEM for an iron particle in Fe/N/CNT showing the (0 0 1) planes of Fe_3C. (f) Digital diffraction pattern of the iron particle shown in (e) highlighting the spots for the (0 0 1) and (2 1 0) planes in Fe_3C.

ICP-OES analyses (see Table 2), respectively, which show that an important fraction of the iron atoms remain in the catalyst bulk rather than at the catalyst surface.

As stated above the XPS analyses indicate the presence of iron oxidized species either as Fe–Nx and/or Fe_3O_4, at the catalyst surface. Taking into account that the presence of the latter species has been ruled out by XAS, the iron species responsible for the XPS peaks are assigned to nitrogen coordinated Fe species similar to those in iron phthalocyanine suggesting that Fe–Nx-like species are the only iron species at the catalysts surface.

The characterization results clearly indicate that the nature of the carbon matrix used for the preparation of Fe/N/C electrocatalysts has a strong influence in the actual nature of the Fe species formed in the final catalysts. The use of graphene-like and CNTs matrixes lead to the stabilization of Fe/Nx ensembles at the catalyst surface. In addition, the nature of carbon material also determines

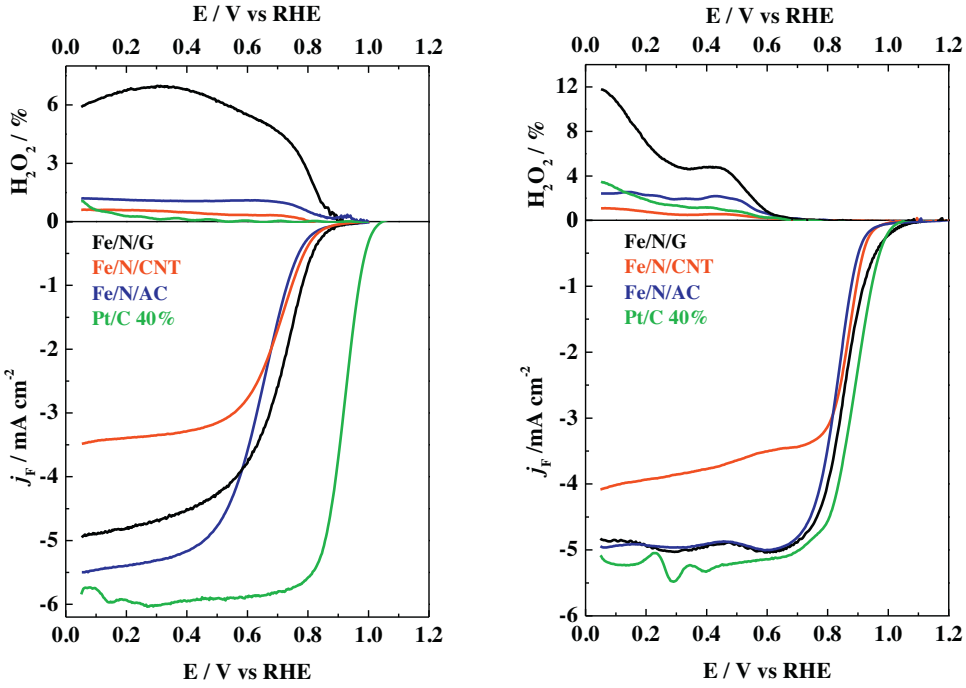

Fig. 5. ORR polarization curves and% H_2O_2 obtained in 0.1 M $HClO_4$ (left panel) and 0.1 M KOH (right panel) with Fe/N/G Fe/N/CNT and Fe/N/AC recorded at 10 mV s^{-1} and 1600 rpm. The performance of Pt/C (40 wt.% from Johnson Matthey) is included for the sake of comparison.

the surface area and textural properties of the catalysts obtained after the pyrolysis step. Hence, the utilization of graphene or active carbon renders Fe/N/C electrocatalysts with higher surface areas than CNTs.

3.2. Catalyst morphology

Representative STEM and TEM images for Fe/N/G and Fe/N/CNT are shown in Fig. 4. Fig. 4a,c shows low magnification images for Fe/N/G and Fe/N/CNT, respectively. The characteristic layers the graphene nanoplates and of the carbon nanotubes can be observed in Fig. 4a,c, respectively, indicating that the structure of the carbon materials used for the synthesis of the catalysts maintained during the synthesis of the catalysts. Representative STEM images for Fe/N/G and Fe/N/CNT are shown as the insets to Fig. 4a,c, respectively. The brighter spots are indicative of the areas containing elements with high *Z* values, *i.e.*, these areas pinpoint the presence of iron particles. Fig. 4b,d shows HR-STEM and HR-TEM micrographs of the iron particles in Fe/N/G and Fe/N/CNT, respectively. As clearly observed in the images, the iron particles are encapsulated within several layers of graphene. The thickness these graphene layers is of *ca.* 3 nm or higher thus preventing the identification of these iron particles by a surface characterization technique such as XPS. As discussed above, EXAFS and XRD analyses indicate the presence of iron carbide (Fe_3C) phases in the catalysts but such species were not detected by XPS. It should be recalled that XRD also fails to indicate the presence of iron nitride (Fe_3N). The nature of the iron particles encapsulated into the graphene layers has been further studied by TEM. Fig. 4e shows a high resolution transmission electron microscopy image for a representative iron particle in Fe/N/CNT. The corresponding digital diffraction pattern is shown in Fig. 4f. The particle was found to lie on the grid oriented along a direction close to the zone axis [−120]. The particle has been indexed according to the unit cell parameters and space group for the Fe_3C structure type. Note that the indexation of this particle for any other crystalline phase of all those present in the Fe–C phase diagram, including the Fe metal itself was not possible.

3.3. Oxygen reduction performance

Fig. 5 shows the ORR polarization curves and hydrogen peroxide yields recorded in 0.1 M $HClO_4$ or 0.1 M KOH with the Fe/N/C catalysts. Irrespectively of the electrolyte, Fe/N/G exhibits the highest activity for the ORR within the range between 0.7 and 1.0 V (*i.e.*, in the kinetically controlled region), followed by Fe/N/CNT and Fe/N/AC.

The ORR can follow two reaction pathways; the so-called 4 electron pathway via the complete reduction of O_2 to H_2O, or the 2 electron pathway where H_2O_2 is formed. As observed in Fig. 5, Fe/N/G records the highest H_2O_2 production of the catalysts under study in both acid and alkaline electrolytes.

The amount of H_2O_2 produced is calculated from Eq. (1). The average number of electrons transferred per O_2 molecule (ne) can be calculated from the H_2O_2 yield calculated from Eq. (2). Thus, Fe/N/G shows a decrease from ne = 4 (no peroxide generation) at 0.75 V to ne = 3.89 at 0.05 V in alkaline media. In acid media, the average number of electron varies from 3.95 at 0.80 V to 3.88 at 0.05 V with a maximum yield of hydrogen peroxide of 7% (ne = 3.86) at 0.30 V. In both cases, the results are very close to the desired value of 4 in line with the results obtained for other non-precious metal catalysts [17]. Fe/N/CNT and Fe/N/AC record lower hydrogen peroxide yields ranging between 1 and 2%, respectively, in both alkaline and acid media.

Fig. 6 shows the mass transport corrected mass activities (i_M) for the Fe/N/C catalysts calculated from Eqs. (3) and (4) recorded in the kinetically controlled region in both acid and alkaline media. The ORR activity trend is more clearly observed, and the i_M for the ORR follows the order Fe/N/G > Fe/N/CNT > Fe/N/AC, irrespectively of the pH of the electrolyte.

The Fe/N/C catalysts reported in this work exhibit higher ORR activity in the alkaline electrolytes, in good agreement with previous results for Fe/N/C based catalysts [41,42]. Although the reason for this fact remains unclear, it is accepted that in alkaline media the ORR is an outer-sphere process whereby the production of H_2O_2 is the predominant reaction pathway [43]. Ramaswamy and Muk-

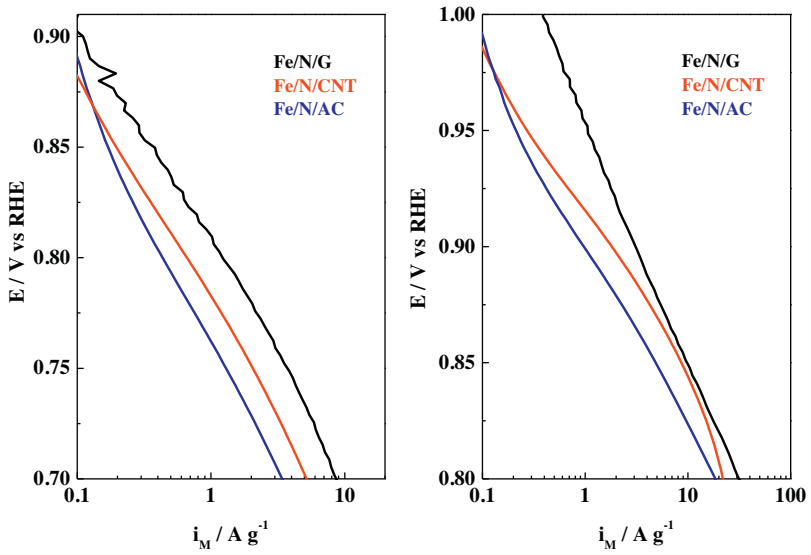

Fig. 6. ORR mass activities in 0.1 M $HClO_4$ (left panel) and 0.1 M KOH (right panel) for the Fe/N/G, Fe/N/CNT and Fe/N/AC recorded at 10 mV s^{-1} and 1600 rpm.

erjee [43] claim that Fe^{2+} sites in Fe/N/C catalysts are capable of stabilizing the peroxide intermediate species in alkaline media, *i.e.*, HO_2^- thus promoting the complete reduction of O_2 to H_2O. On the other hand, Blizanac et al. [44] studied the effect of pH in the ORR with noble metals and concluded that whereas the rate determining step (the transfer of one electron to $O_{2,ad}$ to $O_{2,ad}^-$) is a pH independent process, the reversible potential for the protonation of O_2^- and the formation of peroxide (HO_2^-) is pH dependent. Hence, the thermodynamic potential for peroxide formation shifts to more negative values at alkaline pH and overlaps with the thermodynamic potential of formation of O_2^-. Due to this overlap in equilibrium potentials, the overpotential required to reduce oxygen to peroxide is very low and only weak adsorption of O_2^- in alkaline media is needed to bring the potential of the rate determining step into a useful potential (*vs.* RHE) range.

The mass activity for the ORR in alkaline media with Fe/N/G measured at 0.9 V is of 3.1 ± 0.3 A g^{-1}, or a volumetric activity of 1.25 A cm^{-3} if an effective catalysts density of 0.4 g cm^{-3} is assumed [45]. This value is amongst the highest mass activities reported in literature for similar Fe/N/C based catalysts [17,46,47]. This mass activity value is of only 8 times lower than that recorded with benchmark Pt/C catalyst (Pt 40 wt.%) of 25.8 A g^{-1} at 0.9 V (Fig. S3), a factor that allows to consider Fe/N/G as a feasible alternative to replacing Pt/C catalysts [45]. Moreover, the onset potential (E_{onset}) for the ORR with Fe/N/G, defined as the potential required for generating an ORR current density of 0.1 mA cm^{-2} in a steady-state RDE experiment [12], records a very positive value of 1.04 V, which is close to the best E_{onset} values reported for other Fe/N/C catalysts [17] and higher than the best onset potentials reported for Pt-free or Pt based catalysts in acid media of ca. 1.0 V with Fe- and Co-ordered mesoporous catalysts [16] and single-crystal Pt_3Ni [48] and of 1.05 V with nanoporous PtNi [49]. Also, Fe/N/G and Fe/N/CNT exhibit the same $E_{1/2}$ values of 0.86 V, shifting to 0.83 V for Fe/N/AC. These values are in line with the best $E_{1/2}$ values reported for Fe/N/C-based catalysts for the ORR in alkaline media of 0.86 V (catalyst loading 0.2 mg cm^{-2}) [17].

The question arises as to why Fe/N/G is more active for the ORR than the catalysts prepared with active carbon or carbon nanotubes. In principle, the ORR activity accounts to a combination of the following features, (i) number of active sites, (ii) intrinsic activity of those sites, *i.e.*, the turnover frequency (TOF) and/or (iii) accessibility to the active sites. As discussed above, Fe/N/G and Fe/N/AC exhibit similar BET areas of 415 and 362 m^2 g^{-1}, respectively, which are significantly higher than that of Fe/N/CNT (145 m^2 g^{-1}). On the other hand, all catalysts exhibit similar total N contents and a similar distribution of the N-species. However, the amount of surface Fe in Fe/N/G is 36% lower than in Fe/N/CNT and 22% lower than in Fe/N/AC. These results clearly indicate that the ORR activity is not directly related to the total amount of N or Fe atoms in the catalyst and that the nature of the surface exposed Fe/Nx ensembles actually determines the final performance of the catalysts. According to the X-ray absorption spectra (XANES and EXAFS in Figs. 2 and 3, respectively) Fe/N/G and Fe/N/CNT have higher amount of FeNx like species than Fe/N/AC. Taking into account that most studies coincide in that N-coordinated Fe atoms, typically FeN_4 and/or FeN_{2+2} moieties [36,50], are the most active sites for the ORR [6,36] the higher ORR activity of Fe/N/G and Fe/N/CNT can be ascribed to a higher amount of active sites for the ORR available in those catalysts as compared with the Fe/N/AC counterpart.

3.4. Long term stability tests

Displaying high electrocatalytic activity for the ORR is not the only requirement for NPMCs to replace Pt/C as cathode electrodes of commercial fuel cells. Durability is in fact a serious issue to be addressed with Fe-based electrodes for the ORR [51]. An improved durability both during operation and start up and stop cycles of a fuel cell is an essential feature of a commercial catalyst. A benchmark protocol for O_2 saturated the assessment of stability and durability of Fe/N/C based catalyst has not been reported hitherto. Different groups report different protocols based upon repeated cycling typically between 0.6 and 1.0 V [16,17], or between 0.6 and 1.3 V [52] in N_2 saturated electrolytes. Other protocols are based upon square-wave programs in N_2 saturated electrolytes between 0.9 and 1.4 V [51]. Recently, the DOE recommended to increase the upper potential limit up to 1.4 V in order to better simulate start-up/shutdown processes in a fuel cell [53].

In a first step, the stability of the catalysts was assessed by subjecting all of catalysts to 3000 consecutive cycles between 0.6 and 1.0 V at 50 mV s^{-1} in O_2 saturated 0.1 M KOH. Fig. 7 shows the mass activities (i_M) for Fe/N/G, Fe/N/CNT and Fe/N/AC in the kinetically controlled region before and after the stability tests.

As observed, Fe/N/G and Fe/N/CNT are very stable recording identical i_M at 0.9 V before and after recording 3000 consecutive potential cycles in O_2 saturated electrolytes. On the other hand, Fe/N/AC becomes severely degraded, recording a mass activity loss

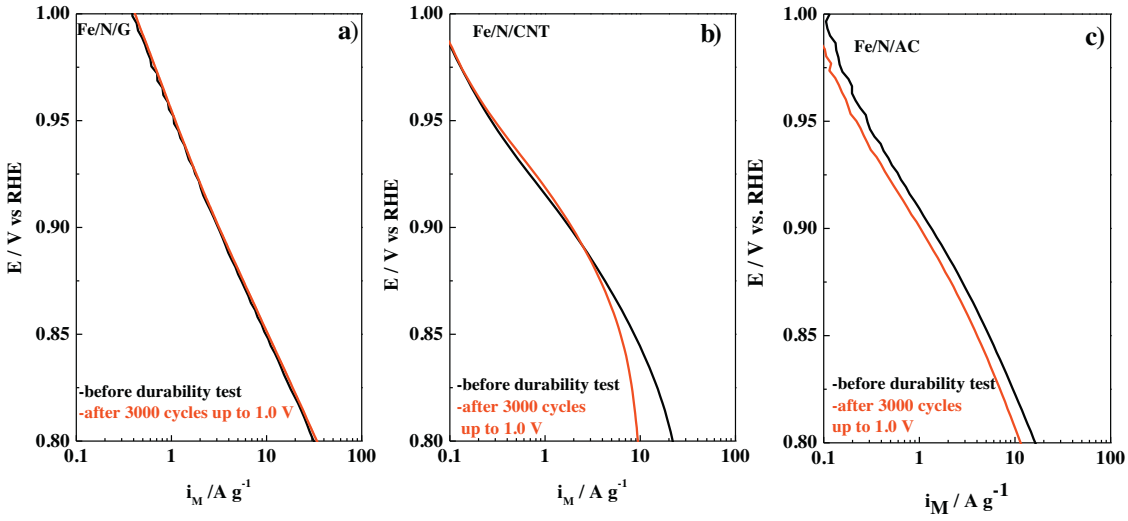

Fig. 7. ORR mass activities in 0.1 M KOH at 10 mV s^{-1} and 1600 rpm for Fe/N/G (a), Fe/N/CNT (b) and Fe/N/AC (c) before (black lines) and after (red lines) the stability tests: 3000 cycles between 0.6 and 1.0 V at 50 mV s^{-1}. (For interpretation of the references to color in this figure legend, the reader is referred to the web version of this article.)

of *ca.* 24% at 0.9 V. The stability of these Fe/N-based catalysts in alkaline electrolyte is higher than that of the benchmark Pt/C (40 wt.%) catalyst which records a severe mass activity loss of *ca.* 64% at 0.9 V after cycling at same conditions (see Fig. S3). The most stable catalysts in alkaline media (Fe/N/G and Fe/N/CNT) were subjected to the same stability test but in acid media (0.1 M $HClO_4$). Fig. S4 shows the mass activities for the catalysts before and after the stability tests. As observed, the stability of, Fe/N/G and Fe/N/CNT in the acidic electrolyte is significantly lower than in the alkaline one showing mass activity losses at 0.9 V of 42% and 54%, respectively.

In view of the high stability of these catalysts, especially Fe/N/G, we have conducted a more severe degradation test which consists in consecutive cycling of the electrode in O_2 saturated alkaline electrolyte between 0.4 and 1.4 V at 1 V s^{-1}. This protocol is similar to that reported for the study of Pt/C catalysts [54], but more severe than those reported recently for Fe/N/C based catalysts [52]. Fig. 8 shows the ORR polarization curves and the mass transport corrected mass activities (i_M) in the kinetically controlled region recorded with Fe/N/G, Fe/N/AC and Fe/N/CNT catalysts in alkaline media before and after the stability test. Again, Fe/N/G exhibits an excellent stability showing almost identical j_F and i_M values within the potential region between E_{onset} and $E = 0.8$ V.

These results suggest that the use of graphene as carbon matrix for the preparation of NPMCs confers unique properties to the final material for ORR in terms of activity and especially in terms of stability. As shown in Fig. 8, the ORR activity of Fe/N/G remains very stable after being subjected to repeated cycling up to potential values of 1.4 V for 3000 consecutive cycles. The mass activity decreases *ca.* 10% after this severe durability test. This value translates into a ΔE of ≈10 mV to less positive values for obtaining a current density of 3.1 A g^{-1} before and after the stability test. When subjected to the same harsh duration test (3000 cycles up to 1.4 V), the Fe/N/CNT catalyst records a severe a mass activity loss of 28% at 0.9 V as shown in Fig. S3. This ORR activity decay is very similar to the one observed for Fe/N/AC catalyst after cycling up to 1.4 V.

To the best of our knowledge this is the first time that such a high stability for the ORR with Fe/N/C based catalysts has been reported under severe degradation conditions, demonstrating the potential benefits of the use of graphene as carbon matrix for the preparation of NPMCs for the ORR in alkaline media.

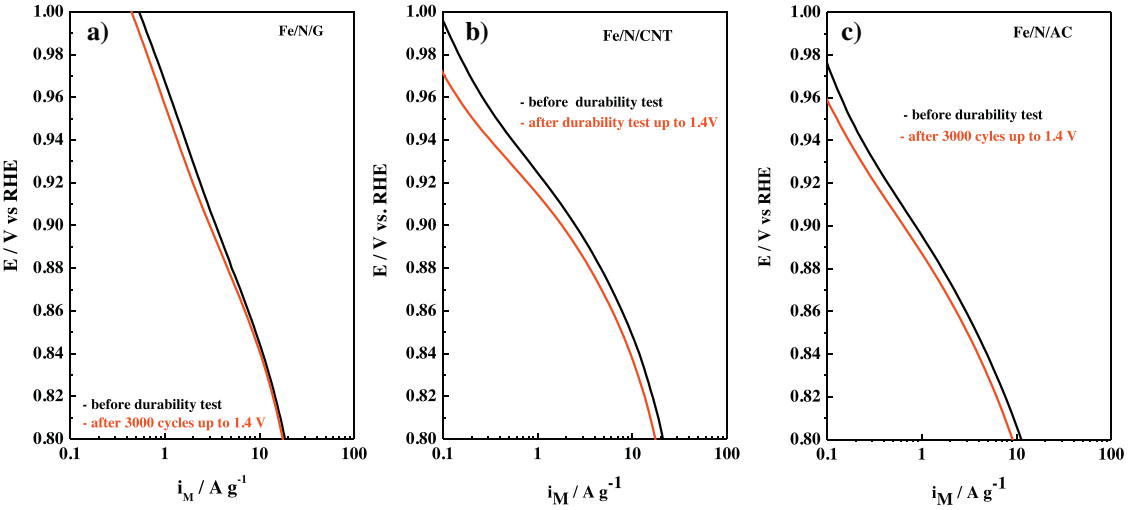

Fig. 8. ORR mass activities for Fe/N/G, Fe/N/CNT and Fe/N/AC catalysts recorded in O_2 saturated 0.1 M KOH at 10 mV s^{-1} and 1600 rpm before (black line) and after (red line) the stability test: 3000 cycles between 0.4 and 1.4 V at 1 V s^{-1}. (For interpretation of the references to color in this figure legend, the reader is referred to the web version of this article.)

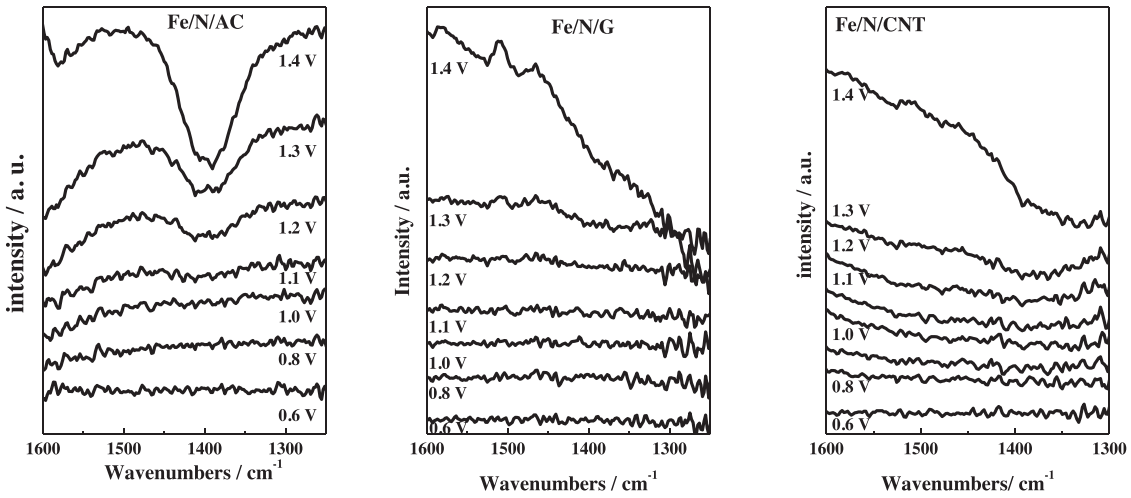

Fig. 9. *In situ* IRRA spectra recorded at different potentials up to 1.4 V in KOH 0.1 M Ar-saturated electrolytes for Fe/N/AC, Fe/N/G and Fe/N/CNT catalysts.

In principle, several effects can contribute to the degradation of Fe/N/C catalysts such as the oxidation of the iron cations coordinated to nitrogen leading to demetallation and/or the elimination of FeNx sites embedded in carbon matrix due to corrosion of the surrounding carbon support [51]. In order to assess whether the higher stability of Fe/N/G catalyst is related to a better resistance against corrosion, we studied the evolution of the catalysts with the applied potential by means of in situ electrochemical infrared reflection adsorption spectroscopy (EC-IRRAS). In principle, carbon corrosion can be monitored by following the evolution of evolved CO_2 with potential. However, CO_2 is not a stable species in alkaline electrolyte forming carbonates at high pH values. Carbonates are characterized by an IR band at *ca.* 1400 cm^{-1}. Note that negative going bands in the IRRA spectra are indicative of the formation of species.

Fig. 9 shows the 1600 and 1250 cm^{-1} region of the IR spectra recorded during the ORR in alkaline electrolyte. A negative going band at 1400 cm^{-1} is clearly observed in the spectra for Fe/N/AC recorded at $E \geq 1.1$ V. This band, which is ascribed to the formation of carbonate species, is indicative of the formation of CO_2 due to the over oxidation of the active carbon at $E \geq 1.1$ V. On the other hand, the spectra recorded for Fe/N/G are featureless, and IR bands indicative of the formation of carbonates (or CO_2) or other oxidized species are not observed. The spectra recorded for Fe/N/CNT resemble to those recorded for Fe/N/G and the formation of carbonate species is not as clearly observed as with Fe/N/AC. Nonetheless, the spectra recorded at $E \geq 1.3$ V show a low intense broad band at *ca.* 1400 cm^{-1} which could be indicative of the incipient formation of carbonates.

In order to verify the formation of CO_2 with the applied potential, the IR spectra were also recorded in acid electrolyte (0.1 M $HClO_4$) under the same experimental conditions. In line with the experiments in alkaline electrolyte, the formation of CO_2 (characterized by an IR band at 2343 cm^{-1}) is clearly observed in the spectra recorded at $E \geq 1.2$ V with Fe/N/AC (Fig. S4). On the other hand, the spectra recorded with Fe/N/G or Fe/N/CNT only show a very low intense band at *ca.* 2343 cm^{-1} ascribed to the formation of CO_2 at $E \geq 1.4$ V and 1.3 V, respectively. This behavior indicates that graphene and CNTs are more stable supports towards corrosion than active carbon. It should be noted that CO_2 formation with CNT is slightly higher than with graphene suggesting that CNTs are more prone to be oxidized than graphene, *i.e.*, they are more stable than AC but less stable than graphene. With these results in mind, and taking into account that the nature of the Fe–Nx sites at the catalyst surface is similar in all catalysts, it is clear that the loss of the catalytic activity of Fe/N/C catalysts is directly related with the stability of the carbon matrix against corrosion (CO_2 formation) than with the stability of the Fe/Nx ensembles. It should be remarked that catalyst deactivation is only observed once carbon corrosion takes place. Therefore, using highly graphitized materials such as graphene-like or, to a lesser extent CNTs, prevents carbon corrosion and as a result the Fe/Nx moieties remain stable at the catalyst surface (see the high ORR stability of Fe/N/G shown in Fig. 8), especially with Fe/N/G. On the contrary, Fe/N/AC is the most prone of the catalysts under study to suffer carbon corrosion through a 4 electron mechanism producing CO_2 (leading to the formation of carbonates in alkaline electrolytes). As a consequence, upon carbon oxidation the Fe/Nx active sites are no longer stable at the catalyst surface probably leaching into the electrolyte. As a consequence the ORR activity of Fe/N/AC drops more significantly than that of Fe/N/G or Fe/N/CNT in which Fe/Nx ensembles remain stable within the resistant carbon matrix. It should be remarked that the stability of the Fe/N/C catalysts is only affected by the stability of the carbon matrix and that once the threshold potential for carbon corrosion is reached a severe loss in the catalytic performance for the ORR is observed regardless of the actual nature of the carbon matrix. Thus, Fe/N/CNT losses *ca.* 29% of its mass activity for the ORR when subjected to potentials above 1.3 V; this value is the onset potential for the corrosion of the CNTs.

Conclusions

This paper shows that the nature of the carbon matrix (graphene, carbon nanotubes or active carbon) is an important parameter for the designing of NPMCs based upon Fe/N/carbon. Catalysts prepared with graphitic materials such as graphene or CNTs result in the preferential formation of FeNx-like species at the catalyst surface and as a result to a higher activity for the ORR in acid and alkaline electrolytes. In addition, graphene is highly resistant towards corrosion at potentials up to 1.4. As a consequence the Fe/Nx ensembles formed on graphene are also extremely stable for the ORR in alkaline media. In fact, the activity of Fe/N/G for the ORR in alkaline electrolyte remains stable even after severe degradation protocol consisting in subjecting the electrode to 3000 consecutive cycles up to 1.4 V.

Acknowledgments

This project was funded by the Deanship of Scientific Research (DSR), King Abdulaziz University, Jeddah, under grant number

(D002/436). The authors, therefore, acknowledge with thanks DSR technical and financial support. Economic support from projects ENE2013-42322-R from the Spanish Ministry of Economy and Competitiveness, and project 201480E122 from the CSIC are also acknowledged. XAS experiments were performed at CLAESS beamline at ALBA Synchrotron with the collaboration of ALBA staff.

Appendix A. Supplementary data

Supplementary data associated with this article can be found, in the online version, at http://dx.doi.org/10.1016/j.apcatb.2015.10.043.

References

[1] Y. Wang, K.S. Chen, J. Mishler, S.C. Cho, X.C. Adroher, A review of polymer electrolyte membrane fuel cells: technology, applications, and needs on fundamental research, Appl. Energy 88 (2011) 981–1007.
[2] G. Girishkumar, B. McCloskey, A.C. Luntz, S. Swanson, W. Wilcke, Lithium–air battery: promise and challenges, J. Phys. Chem. Lett. 1 (2010) 2193–2203.
[3] C.C.L. McCrory, S. Jung, I.M. Ferrer, S.M. Chatman, J.C. Peters, T.F. Jaramillo, Benchmarking hydrogen evolving reaction and oxygen evolving reaction electrocatalysts for solar water splitting devices, J. Am. Chem. Soc. 137 (2015) 4347–4357.
[4] I. Katsounaros, S. Cherevko, A.R. Zeradjanin, K.J.J. Mayrhofer, Oxygen electrochemistry as a cornerstone for sustainable energy conversion, Angew. Chem. Int. Ed. 53 (2014) 102–121.
[5] M.S. Faber, S. Jin, Earth-abundant inorganic electrocatalysts and their nanostructures for energy conversion applications, Energy Environ. Sci. 7 (2014) 3519–3542.
[6] F. Jaouen, J. Herranz, M. Lefèvre, J.P. Dodelet, U.I. Kramm, I. Herrmann, P. Bogdanoff, J. Maruyama, T. Nagaoka, A. Garsuch, J.R. Dahn, T. Olson, S. Pylypenko, P. Atanassov, E.A. Ustinov, Cross-laboratory experimental study of non-noble-metal electrocatalysts for the oxygen reduction reaction, ACS Appl. Mater. Interface 1 (2009) 1623–1639.
[7] F. Jaouen, E. Proietti, M. Lefèvre, R. Chenitz, J.P. Dodelet, G. Wu, H.T. Chung, C.M. Johnston, P. Zelenay, Recent advances in non-precious metal catalysis for oxygen-reduction reaction in polymer electrolyte fuel cells, Energ. Environ. Sci. 4 (2011) 114–130.
[8] M. Lefèvre, E. Proietti, F. Jaouen, J.P. Dodelet, Iron-based catalysts with improved oxygen reduction activity in polymer electrolyte fuel cells, Science 324 (2009) 71–74.
[9] Y. Li, W. Zhou, H. Wang, L. Xie, Y. Liang, F. Wei, J.C. Idrobo, S.J. Pennycook, H. Dai, An oxygen reduction electrocatalyst based on carbon nanotube-graphene complexes, Nat. Nanotechnol. 7 (2012) 394–400.
[10] M. Liu, R. Zhang, W. Chen, Graphene-supported nanoelectrocatalysts for fuel cells: synthesis properties and applications, Chem. Rev. 114 (2014) 5117–5160.
[11] E. Proietti, F. Jaouen, M. Lefèvre, N. Larouche, J. Tian, J. Herranz, J.P. Dodelet, Iron-based cathode catalyst with enhanced power density in polymer electrolyte membrane fuel cells, Nat. Commun. 2 (2011).
[12] G. Wu, K.L. More, C.M. Johnston, P. Zelenay, High-performance electrocatalysts for oxygen reduction derived from polyaniline, iron, and cobalt, Science 332 (2011) 443–447.
[13] G. Wu, P. Zelenay, Nanostructured nonprecious metal catalysts for oxygen reduction reaction, Acc. Chem. Res. 46 (2013) 1878–1889.
[14] Z.S. Wu, S. Yang, Y. Sun, K. Parvez, X. Feng, K. Müllen, 3D nitrogen-doped graphene aerogel-supported Fe_3O_4 nanoparticles as efficient electrocatalysts for the oxygen reduction reaction, J. Am. Chem. Soc. 134 (2012) 9082–9085.
[15] C. Domínguez, F.J. Pérez-Alonso, M. Abdel Salam, J.L. Gómez De La Fuente, S.A. Al-Thabaiti, S.N. Basahel, M.A. Peña, J.L.G. Fierro, S. Rojas, Effect of transition metal (M: Fe, Co or Mn) for the oxygen reduction reaction with non-precious metal catalysts in acid medium, Int. J. Hydrog. Energy 39 (2014) 5309–5318.
[16] J.Y. Cheon, T. Kim, Y. Choi, H.Y. Jeong, M.G. Kim, Y.J. Sa, J. Kim, Z. Lee, T.H. Yang, K. Kwon, O. Terasaki, G.G. Park, R.R. Adzic, S.H. Joo, Ordered mesoporous porphyrinic carbons with very high electrocatalytic activity for the oxygen reduction reaction, Scientific Rep. 3 (2013).
[17] H.T. Chung, J.H. Won, P. Zelenay, Active and stable carbon nanotube/nanoparticle composite electrocatalyst for oxygen reduction, Nat. Commun. 4 (2013).
[18] S. Zhang, H. Zhang, X. Hua, S. Chen, Tailoring molecular architectures of Fe phthalocyanine on nanocarbon supports for high oxygen reduction performance, J. Mat. Chem. A 3 (2015) 10013–10019.
[19] D.W. Wang, D. Su, Heterogeneous nanocarbon materials for oxygen reduction reaction, Energy Environ. Sci. 7 (2014) 576–591.
[20] C. Domínguez, F.J. Pérez-Alonso, M. Abdel Salam, S.A. Al-Thabaiti, A.Y. Obaid, A.A. Alshehri, J.L. Gómez de la Fuente, J.L.G. Fierro, S. Rojas, On the relationship between N content, textural properties and catalytic performance for the oxygen reduction reaction of N/CNT, Appl. Catal. B: Environ. 162 (2015) 420–429.
[21] F. Jaouen, M. Lefèvre, J.P. Dodelet, M. Cai, Heat-treated Fe/N/C catalysts for O2 electroreduction: are active sites hosted in micropores? J. Phys. Chem. B 110 (2006) 5553–5558.
[22] X. Zhou, J. Qiao, L. Yang, J. Zhang, A review of graphene-based nanostructural materials for both catalyst supports and metal-free catalysts in PEM fuel cell oxygen reduction reactions, Adv. Energ. Mater. 4 (2014), n/a-n/a.
[23] A.O. Al-Youbi, J.L. Gómez de la Fuente, F.J. Pérez-Alonso, A.Y. Obaid, J.L.G. Fierro, M.A. Peña, M. Abdel Salam, S. Rojas, Effects of multiwalled carbon nanotube morphology on the synthesis and electrocatalytic performance of Pt supported by multiwalled carbon nanotubes, Appl. Catal. B: Environ. 150-151 (2014) 21–29.
[24] G. Wu, K.L. More, P. Xu, H.L. Wang, M. Ferrandon, A.J. Kropf, D.J. Myers, S. Ma, C.M. Johnston, P. Zelenay, A carbon-nanotube-supported graphene-rich non-precious metal oxygen reduction catalyst with enhanced performance durability, Chem. Commun. 49 (2013) 3291–3293.
[25] C. Zhang, R. Hao, H. Yin, F. Liu, Y. Hou, Iron phthalocyanine and nitrogen-doped graphene composite as a novel non-precious catalyst for the oxygen reduction reaction, Nanoscale 4 (2012) 7326–7329.
[26] P. Chen, T.Y. Xiao, Y.H. Qian, S.S. Li, S.H. Yu, A nitrogen-doped graphene/carbon nanotube nanocomposite with synergistically enhanced electrochemical activity, Adv. Mater. 25 (2013) 3192–3196.
[27] G.-L. Tian, M.-Q. Zhao, D. Yu, X.-Y. Kong, J.-Q. Huang, Q. Zhang, F. Wei, Nitrogen-doped graphene/carbon nanotube hybrids: in situ formation on bifunctional catalysts and their superior electrocatalytic activity for oxygen evolution/reduction reaction, Small 10 (2014) 2251–2259.
[28] R. Zhang, S. He, Y. Lu, W. Chen, Fe, Co N-functionalized carbon nanotubes in situ grown on 3D porous N-doped carbon foams as a noble metal-free catalyst for oxygen reduction, J. Mater. Chem. A 3 (2015) 3559–3567.
[29] C.D. Wagner, L.E. Davis, M.V. Zeller, J.A. Taylor, R.H. Raymond, L.H. Gale, Empirical atomic sensitivity factors for quantitative analysis by electron spectroscopy for chemical analysis, Surf. Interface Anal. 3 (1981) 211–225.
[30] K.V. Klementev, Extraction of the fine structure from X-ray absorption spectra, J. Phys. D: Appl. Phys. 34 (2001) 209.
[31] U.A. Paulus, T.J. Schmidt, H.A. Gasteiger, R.J. Behm, Oxygen reduction on a high-surface area Pt/vulcan carbon catalyst: a thin-film rotating ring-disk electrode study, J. Electroanal. Chem. 495 (2001) 134–145.
[32] J.R. Pels, F. Kapteijn, J.A. Moulijn, Q. Zhu, K.M. Thomas, Evolution of nitrogen functionalities in carbonaceous materials during pyrolysis, Carbon 33 (1995) 1641–1653.
[33] T. Herranz, S. Rojas, M. Ojeda, F.J. Pérez-Alonso, P. Terreros, K. Pirota, J.L.G. Fierro, Synthesis, structural features, and reactivity of Fe–Mn mixed oxides prepared by microemulsion, Chem. Mater. 18 (2006) 2364–2375.
[34] M. Muhler, R. Schlögl, G. Ertl, The nature of the iron oxide-based catalyst for dehydrogenation of ethylbenzene to styrene 2. Surface chemistry of the active phase, J. Catal. 138 (1992) 413–444.
[35] A.P. Grosvenor, B.A. Kobe, M.C. Biesinger, N.S. McIntyre, Investigation of multiplet splitting of Fe 2p XPS spectra and bonding in iron compounds, Surf. Interface Anal. 36 (2004) 1564–1574.
[36] U.I. Kramm, J. Herranz, N. Larouche, T.M. Arruda, M. Lefèvre, F. Jaouen, P. Bogdanoff, S. Fiechter, I. Abs-Wurmbach, S. Mukerjee, J.P. Dodelet, Structure of the catalytic sites in Fe/N/C-catalysts for O_2-reduction in PEM fuel cells, Phys. Chem. Chem. Phys. 14 (2012) 11673–11688.
[37] U. Tylus, Q. Jia, K. Strickland, N. Ramaswamy, A. Serov, P. Atanassov, S. Mukerjee, Elucidating oxygen reduction active sites in pyrolyzed metal-nitrogen coordinated non-precious-metal electrocatalyst systems, J. Phys. Chem. C 118 (2014) 8999–9008.
[38] H.R. Byon, J. Suntivich, E.J. Crumlin, Y. Shao-Horn, Fe–N-modified multi-walled carbon nanotubes for oxygen reduction reaction in acid, Phys. Chem. Chem. Phys. 13 (2011) 21437–21445.
[39] D. Singh, J. Tian, K. Mamtani, J. King, J.T. Miller, U.S. Ozkan, A comparison of N-containing carbon nanostructures (CNx) and N-coordinated iron–carbon catalysts (FeNC) for the oxygen reduction reaction in acidic media, J. Catal. 317 (2014) 30–43.
[40] H. Meng, N. Larouche, M. Lefèvre, F. Jaouen, B. Stansfield, J.-P. Dodelet, Iron porphyrin-based cathode catalysts for polymer electrolyte membrane fuel cells: effect of NH_3 and Ar mixtures as pyrolysis gases on catalytic activity and stability, Electrochim. Acta 55 (2010) 6450–6461.
[41] C. Domínguez, F.J. Pérez-Alonso, J.L. Gómez De La Fuente, S.A. Al-Thabaiti, S.N. Basahel, A.O. Alyoubi, A.A. Alshehri, M.A. Peña, S. Rojas, Influence of the electrolyte for the oxygen reduction reaction with Fe/N/C and Fe/N/CNT electrocatalysts, J. Power Sources 271 (2014) 87–96.
[42] N. Ramaswamy, S. Mukerjee, Fundamental mechanistic understanding of electrocatalysis of oxygen reduction on Pt and non-Pt surfaces: acid versus alkaline media, Adv. Phys. Chem. 2012 (2012).
[43] N. Ramaswamy, S. Mukerjee, Influence of inner- and outer-sphere electron transfer mechanisms during electrocatalysis of oxygen reduction in alkaline media, J. Phys. Chem. C 115 (2011) 18015–18026.
[44] B.B. Blizanac, P.N. Ross, N.M. Markovic, Oxygen electroreduction on Ag(111): the pH effect, Electrochim. Acta 52 (2007) 2264–2271.
[45] H.A. Gasteiger, S.S. Kocha, B. Sompalli, F.T. Wagner, Activity benchmarks and requirements for Pt, Pt-alloy, and non-Pt oxygen reduction catalysts for PEMFCs, Appl. Catal. B Environ. 56 (2005) 9–35.
[46] M. Piana, S. Catanorchi, H.A. Gasteiger, Kinetics of non-Platinum group metal catalysts for the oxygen reduction reaction in alkaline medium, ECS Trans. 16 (2008) 2045–2055.

[47] H. Meng, F. Jaouen, E. Proietti, M. Lefèvre, J.P. Dodelet, pH-effect on oxygen reduction activity of Fe-based electro-catalysts, Electrochem. Commun. 11 (2009) 1986–1989.
[48] V.R. Stamenkovic, B. Fowler, B.S. Mun, G. Wang, P.N. Ross, C.A. Lucas, N.M. Markovic, Improved oxygen reduction activity on $Pt_3Ni(111)$ via increased surface site availability, Science 315 (2007) 493–497.
[49] J. Snyder, T. Fujita, M.W. Chen, J. Erlebacher, Oxygen reduction in nanoporous metal–ionic liquid composite electrocatalysts, Nat. Mater. 9 (2010) 904–907.
[50] J. Herranz, F. Jaouen, M. Lefèvre, U.I. Kramm, E. Proietti, J.P. Dodelet, P. Bogdanoff, S. Fiechter, I. Abs-Wurmbach, P. Bertrand, T.M. Arruda, S. Mukerjee, Unveiling N-protonation and anion-binding effects on Fe/N/C catalysts for O_2 reduction in proton-exchange-membrane fuel cells, J. Phys. Chem. C 115 (2011) 16087–16097.
[51] V. Goellner, C. Baldizzone, A. Schuppert, M.T. Sougrati, K. Mayrhofer, F. Jaouen, Degradation of Fe/N/C catalysts upon high polarization in acid medium, Phys. Chem. Chem. Phys. 16 (2014) 18454–18462.
[52] N. Ranjbar Sahraie, J.P. Paraknowitsch, C. Göbel, A. Thomas, P. Strasser, Noble-metal-free electrocatalysts with enhanced ORR performance by task-specific functionalization of carbon using ionic liquid precursor systems, J. Am. Chem. Soc. 136 (2014) 14486–14497.
[53] P. Zelenay, Non-PGM Target Update, 2015. http://energy.gov/sites/prod/files/2014/07/f17/fcto_cwg_june2014_zelenay.pdf.
[54] J.C. Meier, I. Katsounaros, C. Galeano, H.J. Bongard, A.A. Topalov, A. Kostka, A. Karschin, F. Schuth, K.J.J. Mayrhofer, Stability investigations of electrocatalysts on the nanoscale, Energy Environ. Sci. 5 (2012) 9319–9330.